Journal of Nuclear Materials 392 (2009) 45–54

Contents lists available at ScienceDirect

Journal of Nuclear Materials

journal homepage: www.elsevier.com/locate/jnucmat

Corrosion of irradiated MOX fuel in presence of dissolved H_2

P. Carbol [a,*], P. Fors [a,b], S. Van Winckel [a], K. Spahiu [b]

[a] European Commission, Joint Research Centre, Institute for Transuranium Elements, P.O. Box 2340, 76125 Karlsruhe, Germany
[b] Chalmers University of Technology, Chemical and Biological Engineering, Nuclear Chemistry, 41296 Göteborg, Sweden

ARTICLE INFO

Article history:
Received 26 November 2008
Accepted 12 March 2009

ABSTRACT

The corrosion behaviour of irradiated MOX fuel (47 GWd/tHM) has been studied in an autoclave experiment simulating repository conditions. Fuel fragments were corroded at room temperature in a 10 mM NaCl/2 mM $NaHCO_3$ solution in presence of dissolved H_2 for 2100 days. The results show that dissolved H_2 in concentration 1 mM and higher inhibits oxidation and dissolution of the fragments. Stable U and Pu concentrations were measured at 7×10^{-10} and 5×10^{-11} M, respectively. Caesium was only released during the first two years of the experiment. The results indicate that the UO_2 matrix of a spent MOX fuel is the main contributor to the measured dissolution, while the corrosion of the high burn-up Pu-rich islands appears negligible.

1. Introduction

Direct disposal of spent nuclear fuel in deep geological formations is being considered by several countries [1]. In most European concepts for disposal of high-level waste, spent nuclear fuel will be encapsulated in canisters containing large amounts of iron. The canisters will be placed in several hundred meters deep repositories, built in granitic bedrock, clay or salt formations. In the granite repository, the canisters will be surrounded by compacted bentonite clay. In this concept, the advantage of a multiple barrier system to isolate the waste from the biosphere for a very long time is emphasized [2].

The most significant pathway for mobilization of radionuclides from the spent fuel and subsequent migration to the biosphere includes corrosion and transport by groundwater. The multi-barrier system is designed to prevent groundwater from coming into contact with the fuel. In case of multi-barrier failure, it is necessary to estimate the release rates of the radionuclides from the spent fuel, the so-called source term. The source term in a water-saturated medium is normally described as a combination of two terms [3]:

- possible instantaneous release of safety relevant radionuclides from the fuel (mainly ^{135}Cs and ^{129}I) and fuel assembly materials (mainly ^{14}C and ^{36}Cl) at the time of containment failure (instant release fraction).
- Slow long-term release, corresponding to the dissolution of the UO_2 matrix.

The instant release fraction depends on the burn-up, but is considered to be small (a few percent) for a normal burn-up (45 GWd/tHM) UO_2 fuel. The majority of radionuclides will be released when the UO_2 matrix dissolves, which strongly depends on the redox conditions of the groundwater in contact with the fuel.

Minerals and bacteria will consume free oxygen present in the repository at the time of its closure and reducing conditions will prevail in the repository after a few years [4]. In the case of groundwater intrusion, the anoxic water will corrode the container iron and large amounts of H_2 will be produced through the reaction [5]:

$$3Fe(s) + 4H_2O \rightarrow Fe_3O_4(s) + 4H_2(g).$$

The H_2 concentration at the fuel surface will depend on the rate balance between the H_2 production and its loss by diffusive mass transport out of the container. If the rate of diffusive mass transport of H_2 is limited, e.g., when the hole in the canister caused by corrosion is small, the concentration of dissolved H_2 is expected to exceed its solubility in groundwater [6].

Although reducing conditions will generally prevail in the repository, local oxidizing conditions are expected near the spent fuel surface due to oxidizing species produced by radiolysis of water [7]. These oxidizing species might accelerate the dissolution of the UO_2 matrix. A number of studies of the effect of radiation induced oxidizing conditions near a fuel surface in otherwise reducing, H_2 saturated surroundings, have been carried out in recent years [7–11]. A summary of the results from some of these experiments, and, as a reference, one experiment conducted without H_2 (in air), is presented in Table 1.

The main outcome of these studies is that the presence of H_2 lowers the concentration of dissolved U in solution by several orders of magnitude. Several recent studies have proposed mechanisms based on the catalytic effect of metallic ε-particles (composed of the fission products Mo, Pd, Tc, Rh and Ru [12]) on the H_2 activation at the fuel surface. The corrosion potential of SIMFUEL pellets decreased proportionally with hydrogen

* Corresponding author. Tel.: +49 7247 951 178; fax: +49 7247 951 591.
E-mail address: paul.carbol@ec.europa.eu (P. Carbol).

0022-3115/$ - see front matter © 2009 Elsevier B.V. All rights reserved.
doi:10.1016/j.jnucmat.2009.03.044

Table 1
Uranium concentrations in solution together with experimental parameters for reported corrosion experiments on irradiated UO_2 fuel.

	Burn-up (GWd/tHM)	H_2 (MPa)	Temperature (°C)	pH	Corrosion time (d)	Concentration U (M)	Autoclave material	Solution
In air								
Forsyth [44]	42	0	25	8.2	1083	1×10^{-5}	Pyrex flask	Synthetic groundwater
With H_2								
Spahiu 2000 [11]	43	5.0	70	~8.5	312	1×10^{-10}	Stainless steel	10 mM NaCl/2 mM $NaHCO_3$
Spahiu 2000 [11]	43	5.0	25	~8.5	~50	5×10^{-9}	Stainless steel	10 mM NaCl/2 mM $NaHCO_3$
Albinsson 2003 [9]	41	1.0	25	8.1	21	5×10^{-9}	PEEK	Mod. Allard + Fe strip
Spahiu 2004 [8]	43	0.5	70	~8.5	376	2×10^{-10}	Quartz	10 mM NaCl/2 mM $NaHCO_3$
Loida 2005 [7]	50	0.32	25	7.8	1095	1×10^{-8}	Ti/Pd	5.6 mol NaCl (kg H_2O)$^{-1}$
Loida 2005 [7]	50	0.28	25	9.5	1619	1×10^{-8}	Ti/Pd	5.6 mol NaCl (kg H_2O)$^{-1}$ + Fe powder

concentration to very low values corresponding to those of the $H_2/2H^+$ couple [13]. Studies of the catalytic effect of pure Pd particles on the reaction between H_2 and H_2O_2 show that the reaction is very fast, practically diffusion controlled and independent of the H_2 pressure in the range 1–40 bar [14]. Based on the decrease of the corrosion potential reported in [13], a solid phase reduction of oxidized $U(VI)_{surf}$ mediated by hydrogen via ε-particles has been proposed [15]. Long term fuel dissolution experiments in closed systems [16] indicate that the rate of fuel dissolution is approaching zero for radiolytically produced H_2 concentrations in the range 10^{-5} to 10^{-4} M. The proposed surface reduction process on ε-particles has successfully been used to model this result [17]. However, the results obtained with highly doped UO_2 pellets in the presence of H_2 [18] and the results from our laboratory [19] indicate that an additional mechanism applies also in the absence of ε-particles.

Corrosion experiments in presence of H_2 have, so far, only been made on spent UO_2 fuels although several thousand MOX fuel assemblies have been irradiated in European reactors [20]. In order to complete the performance assessments for the final repositories there is a need to obtain corrosion data for spent MOX fuels under reducing conditions [3].

Historically, the driving force for production of MOX and its use as fuel was to control the accumulation of ^{239}Pu and ^{241}Pu produced during irradiation of UO_2 and to ensure a more efficient use of the fuel. The reprocessing of spent nuclear fuel, necessary to separate U and Pu from the rest of the fuel (fission products and other actinides), has been carried out since the late 1950s. The original plan was to use the separated Pu as fuel in fast breeder reactors [21]. However, the present recycling option for separated Pu is fabrication of MOX fuel, which is burned in light water reactors (LWR). Irradiation of MOX fuel in a LWR is efficient in decreasing the total Pu content by 30%. However, the Pu composition shifts towards heavier non-fissile isotopes. This limits the practical reprocessing of Pu in LWR to one cycle [21]. Mono-recycle burning of the Pu decreases the number of fuel assemblies to be stored in the final repository [21,22]. Consequently, reprocessing of spent nuclear fuel has continued after termination of the fast reactor programs and a large amount of MOX fuel for LWR burning is annually fabricated in France and the UK.

As a consequence of the mono-recycling limitation for MOX fuel, basically two routes are considered for the back end of spent MOX assemblies: further reprocessing and use as energy source in future reactor types, or direct disposal as waste in a final repository. France considers spent MOX fuel as an energy resource and plans to reprocess it in the future [22]. Other countries, such as Sweden, Spain, Germany and Finland, which have no plans to build fast reactors in the future, have decided to dispose of spent MOX fuel in geologic repositories without reprocessing.

As alluded to above, the latter route requires understanding of the long-term behaviour of spent MOX fuel under repository conditions. A few matrix corrosion studies under oxidizing conditions have been published for MOX fuels [23–26]. Since oxidative dissolution takes place in these studies, the release of matrix elements U and Pu is relatively high; however, during long term static leaching experiments, it becomes limited by the solubility of secondary phases formed during the test, thus making it complicated to determine true matrix dissolution rates. The reported release rate of strontium, a non redox-sensitive matrix bound fission product, seems to be considerably higher from MOX fuel than from UO_2 of similar average burn-up. The values given in literature indicate a factor of 2 [23] to 7 [25] times higher strontium release rates from MOX. This difference raises a question as to the specific behaviour of spent MOX fuel in case of canister failure and exposure to groundwater in a repository.

To address this problem and examine the corrosion behaviour of spent MOX fuel in contact with groundwater under deep granitic bedrock conditions, an experiment was set up. The experiment aimed at verifying H_2 driven inhibition of MOX fuel dissolution at different concentrations of dissolved H_2, and to identify differences and similarities in MOX and UO_2 corrosion.

2. Materials and methods

2.1. Fuel

The MOX fuel used in this study was fabricated by the optimized co-milling process (OCOM). Fuel manufactured by this process has a duplex structure and consists of Pu-rich agglomerates up to 200 μm in size dispersed in a matrix of natural UO_2 containing a small addition of MOX fuel scrap [27]. The Pu content in the agglomerates corresponded to 30 wt% (here this fuel is referred to as OCOM 30) giving an average Pu concentration in the fuel of 4.9 wt%.

During the irradiation, ~75% of the fissions occur in the Pu-rich agglomerates (calculation based on data from [28]). This creates an uneven burn-up, and therefore, an uneven fission product distribution in the fuel. The high local burn-up in the agglomerates (up to 270 GWd/tHM [28]) results in a microstructure of fine grains and large pores with a diameter of several microns [29], which is similar to the rim structure formed on UO_2 fuels at local burn-ups above 60-80 GWd/tHM [27]. Relevant properties and irradiation data for the OCOM 30 fuel used in our corrosion experiment are given in Table 2.

The fuel was irradiated in four consecutive cycles in the pressurized water reactor at the Obrigheim nuclear power station (KWO) with start in July 1986. The rod from which the fuel was cut (PN20) was placed at a central position of the 14 × 16 fuel rods assembly and was irradiated under normal conditions during all four cycles, i.e., without ramping. The average linear power did not exceed 23 kW · m^{-1}. Hence, the fuel centre temperature barely exceeded 1300 °C [28]. As a consequence, the duplex structure produced during fabrication remained after irradiation [30].

Table 2
Fuel and irradiation data of the rod PN20 segment P504 [45].

Parameters	
Fuel data	
Fuel	UO_2–4.92 wt% PuO_2
Fissile fractions	0.72 wt% $^{235}U/U_{total}$, 71.1 wt% $^{239,241}Pu/Pu_{total}$
Pu fraction in agglomerates	Pu/(U + Pu) = 30%
Fuel stoichiometry	1.995
Fuel density	10.46 kg/dm^3
Pellet diameter	9.13 mm
Pellet length	11.25 mm
Average grain size	9 μm
Fuel pin data	
Radial gap	0.085 mm
Fuel pin diameter	10.75 mm
Cladding thickness	0.725 mm
Cladding material	Zircaloy-4
Internal pre-pressure	22.5 bar (room temperature)
Irradiation data	
Total number of irradiation days	1246 EFPD
Number of irradiation cycles	4
Average linear power	20.8 kW/m (maximum 23 kW/m)
Mean outer cladding temperature	320 °C
Average fuel burn-up	44.4 GWd/tHM

From PN20 a sub-segment, P504, was selected for post-irradiation examination (PIE). This segment had a flat axial burn-up profile, as determined by γ-scanning, and a fuel burn-up of 47.5 GWd/tHM which was higher than the average rod burn-up of 44.4 GWd/tHM. Oxygen potential measurements of the irradiated MOX fuel segment showed that it was $UO_{2.00}$. The post-irradiation characterization revealed a fuel matrix with a homogenous distribution of Pu agglomerates. The fuel grain size varied slightly with distance from the centre. Most grains, however, were found to be in the range 4-7 μm, i.e., smaller than in the un-irradiated fuel. Both fine and coarse porosity was observed in the fuel matrix as a result of the high burn-up in the Pu agglomerates. A total dissolution of the fuel was made and the content of the actinides and fission products analyzed. The results, mainly the ^{148}Nd-isotope and the Pu-vector, were used for an ORIGEN calculation [31] of the complete fuel inventory. The specific activities of the main fission products and actinides are given in Table 3.

A 1.1 mm thick disc was cut from fuel segment P504 under nitrogen atmosphere (<2 vol.% O_2). Prior to cutting the fuel disc, the cutting plan of segment P504 was examined to avoid including gaps between adjacent pellets in the sample. The fuel slice with its Zircaloy-4 cladding and the de-cladded fuel fragments are shown in Fig. 1. The gap between the fuel and the Zircaloy-4 cladding was closed during irradiation, as is evident in Fig. 1(a). Significant mechanical pressure was needed to detach the fuel from the cladding. Fragments B4 and B5 (Fig. 1(b)) were selected and used in the corrosion experiment. Their total geometric surface area was determined by optical microscopy to be 50.8 mm^2 and their total weight was 0.399 g. The average α-dose rate from the fragments

Table 3
Specific activities of the main fission products and actinides in the irradiated MOX fuel as obtained by the ORIGEN calculation (as of 18 December 2002).

Fission products (Bq/g UO_2)		Actinides (Bq/g UO_2)			
^{90}Sr	1.5×10^9	^{234}U	2.1×10^4	^{241}Pu	1.1×10^{10}
^{125}Sb	1.3×10^7	^{235}U	1.8×10^2	^{242}Pu	5.3×10^1
^{134}Cs	1.3×10^8	^{236}U	1.8×10^3	^{241}Am	3.7×10^8
^{135}Cs	4.6×10^4	^{238}U	9.5×10^3	^{242m}Am	4.0×10^6
^{137}Cs	3.5×10^9	^{237}Np	1.0×10^4	^{243}Am	7.9×10^6
^{144}Ce	4.9×10^5	^{238}Pu	5.7×10^8	^{242}Cm	8.4×10^3
^{154}Eu	2.0×10^8	^{239}Pu	2.4×10^7	^{244}Cm	1.4×10^9
		^{240}Pu	8.0×10^7		

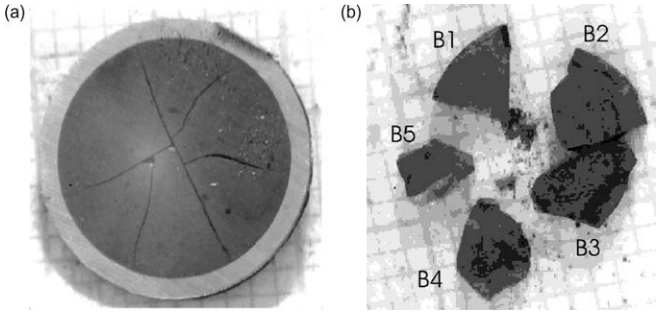

Fig. 1. The fuel for the corrosion experiment extracted from rod PN20. (a) The freshly cut fuel disc with its Zircaloy-4 cladding; (b) the fuel fragments after de-cladding.

to the surrounding solution was calculated to be 1 Gy/s (using the method outlined by Nielsen and Jonsson [32]). Based on the burn-up of 270 GWd/tHM measured in the Pu agglomerates [28], the maximal dose rate is approximately 6 Gy/s. No annealing or other treatment of the fuel was made prior to the corrosion experiment.

2.2. Leachant

The leachant consisted of 10 mM NaCl with 2 mM $NaHCO_3$. The composition has been chosen to mimic a low-saline granitic groundwater. Cations as Ca^{2+} and Mg^{2+} have been excluded from the leachant to avoid the decrease of dissolution rates and/or potential formation of secondary uranyl phases [33,34]. Ultra pure mQ-water, >18 MΩ/m, (PureLab Ultra, Elga LabWater Ltd., UK) and suprapure grade chemicals (Merck GmbH, Germany) were used throughout the experiment.

2.3. Autoclave system

The corrosion experiment was carried out in a two autoclave system (Parr Instruments Co., USA). The first autoclave, denoted experiment autoclave, was placed inside a hot cell, and the second autoclave, denoted refill autoclave, was placed in a glove box connected to the hot cell. The autoclaves had a volume of 200 and 250 cm^3, respectively. The hot cell and the glove box are both run under air atmosphere. A schematic drawing of the autoclave setup is shown in Fig. 2.

Both autoclaves were made of titanium (quality grade II-weldable) with a composition of 99.3 wt% Ti, 0.3 wt% Fe and trace elements: C, N, O and H. All wetted surfaces of the experiment autoclave i.e., pellet holder, magnetic stirrer, valves, security valves and tubing were made of titanium. Graphite gaskets were used to avoid metals that exhibit a high sorption of actinides and organic materials that have poor radiation resistance. A welded tube without filters was used for solution transfer from the refill autoclave to the experiment autoclave.

The experiment autoclave was adapted for hot cell manipulator handling, and certified for a maximal H_2-pressure of 6.8 MPa. The setup allowed the leachant to be purged with gas during fuel loading, and leachant sampling without oxygen intrusion. The refill autoclave setup allowed all gas lines in the entire system to be purged without oxygen intrusion into the experiment autoclave. Each autoclave was connected to a gas bottle (H_2 6.0 or Ar 6.0, Linde/AGA GmbH, Germany), to facilitate purging and solution transfer.

The leachant was sampled through a diving tube with an opening 8 mm above the bottom of the experiment autoclave. The overpressure in the autoclave was utilized to force leachant into 20-ml polyethylene (PE) sampling vials inside the hot cell. The weight of

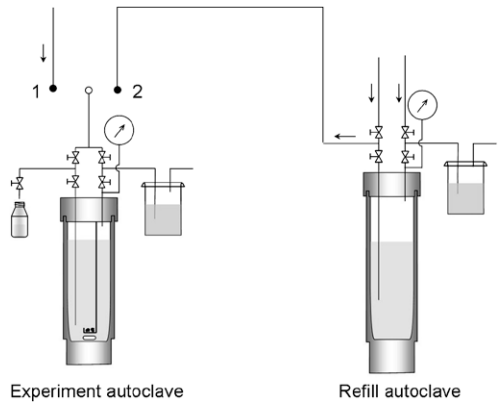

Fig. 2. Schematic of the autoclave setup. The experiment autoclave can be connected to a gas bottle located outside the hot cell (1) or to the refill autoclave located in a glove box (2).

the sampled leachate was recorded on all sampling occasions. Subsequently, the leachate was transferred without filtration into 20-ml liquid scintillation counting vials (polypropylene) outside the hot cell. Finally, the leachates were divided into sub-samples for further analyses.

Leachates were sampled on 18 occasions: after 210 min, and after 1, 26, 203, 492, 653, 734, 1002, 1161, 1283, 1542, 1674, 1850, 1853, 1863, 1976, 2037 and 2078 days. The leachant sampling method was changed during the course of the experiment. On the two first sampling events single aliquots were taken. From then on, a rinse sample was taken to collect the stagnant phase in the sampling tube before taking the actual autoclave leachant sample.

2.4. ICP–MS measurements

Inductively coupled plasma mass spectrometry, ICP–MS (Thermo Element2, Thermo Electron Corporation, Germany), measurements were made on all samples to determine the concentration of the elements shown in Table 4.

A standard ICP–MS operating procedure was followed. All samples were analyzed in duplicates, one with and one without internal standard addition. The elements Sc, Co, In and Ho, and the isotope ^{236}U were used as internal standards. All samples were acidified to 1 M HNO_3. At the start of each measurement, a multi-element calibration was made using certified standards (Agilent Life Sciences/Chemical Analysis GmbH, Germany). Owing to incompatibility of different matrix solutions, the elements of interest were divided into two separate standards. Calibration standards with the concentrations 0, 50, 200, 1000, 5000 and 20 000 ppt were prepared. Two quality-check (QC) solutions, each containing 0.5 ppb of one of the multi-element standards plus 1 ppb of the internal standard, were run to examine the ICP–MS performance. The QC solutions were measured in the beginning of each campaign, after every 15th measured sample, and at the end of each campaign. An instrument blank sample was run every sixth sample to check for memory effects.

The raw data were corrected for internal standard fluctuations. An instrument blank was calculated from all blank measurements. Data that showed contamination or memory effects from previous measurements were discarded to obtain the lowest possible blank concentration. All calibration measurements and samples, including the sample blanks, were corrected for the instrument blank. A sensitivity factor (counts/ppb) was calculated for each isotope in the multi-element standard. To assure zero intercept, the sensitivity factor was based on the average of 1-point calibrations made for each concentration of the standard solutions. By doing this, each standard became equally important. All obviously diverging 1-point calibration values were excluded.

The sensitivity factors were used to calculate the sample concentrations. The concentrations were corrected for dilution during sample preparation, and the average concentration in the sample with and without internal standard was calculated. If some elements in one of the duplicate samples showed clear signs of external contamination these values were excluded. Corrections for mass interferences were made taking also the different sensitivity factors of the interfering isotopes into account. Elemental concentrations were determined for each element of interest. The limit of detection for actinides was approximately 1.0×10^{-12} M whereas the transition elements and lanthanides had a limit of detection of 1.0×10^{-11} M.

Table 4
Elements analyzed by ICP–MS.

Elements	
Transition elements	Ti, V, Cr, Mn, Fe, Ni, Cu, Zn
Fission products	Rb, Sr, Zr, Mo, Tc, Ru, Ag, Cd, Sn, Te, Cs, Ba
Lanthanides	La, Ce, Pr, Nd, Sm, Eu, Gd, Tb, Dy
Actinides	U, Np, Pu, Am, Cm

2.5. γ-Spectrometry measurements

The concentration of the γ-emitters in the leachates were measured using γ-spectrometry. Measurements of leachates and backgrounds were made using a high-purity Ge-detector in 2π-geometry (EG&G Ortec Inc., USA). The detector was energy and efficiency calibrated using certified, mixed nuclide γ-sources (LF199 and PD954, AEA Technology QSA GmbH, Germany). The calibration sources had the geometry of a 2 cm^3 glass vial. The calibration was made at a fixed distance of 1 mm above the detector. The limit of detection of the γ-spectrometry system depends on a number of parameters, but is in general in the range of 0.1 Bq.

A weight-controlled amount of 50–100 mg leachate was transferred to a 2 cm^3 glass vial and the vial was filled with mQ-water to obtain the calibration geometry. The glass vial containing the leachate was measured at the same distance as the calibration sources. The samples were measured for a time period varying between 2.0×10^4 and 1.5×10^6 s. The background was measured for 5.0×10^6 s. The densities of the samples and the calibration sources were similar. The reference date was 18 December 2002.

2.6. Determination of H_2O_2

The concentration of H_2O_2 was determined by absorption spectroscopy using the Ghormley method [35]. This method is based on oxidation of I^- ions by hydrogen H_2O_2 and subsequent absorption measurement at 350 nm of the oxidized I_3^- complex. The absorption measurements were made using a USB2000 spectrometer (Ocean Optics Inc., USA). The detection limit for H_2O_2 in mQ-water was determined to be 5×10^{-9} M for the setup used. However, the limit of detection for H_2O_2 in a 10 mM NaCl + 2 mM $NaHCO_3$ reference solution that had been pressurized with 0.3 MPa Ar-gas in a Ti-autoclave for 6-months was found to be around 1×10^{-6} M due to interfering absorption by dissolved metal ions.

2.7. Sorption

The influence of adsorption on the walls of the sampling PE-vial was examined during the sampling on day 1283. A 1.9 ml portion

of a total 3.4 ml sample was transferred, a few minutes after sampling, into a new PE-vial. By doing this the contact surfaces of PE-vials for the transferred aliquot were doubled in comparison to the leachate remaining in the first PE-vial. The transferred sample was filtered through a 0.2 μm Sterile Acrodisc® filter (Pall Gelman Sciences Co., USA) to avoid fuel particles from influencing the result. The increased sorption surface on the filter was disregarded in the calculations.

The measured U concentrations in the 1xPE sample, and in the 2xPE sample were 8.2×10^{-10} and 7.0×10^{-10} M, respectively. This shows that approximately 2.0×10^{-13} mole U sorbs onto a 20-ml PE-bottle (in a carbonate containing leachate with U concentrations around 8×10^{-10} M). The amount of adsorbed Pu and Tc on the PE-vial was found to be 5.0×10^{-14} moles and 1.8×10^{-14} moles, respectively. The amount of U, Pu and Tc adsorbed onto a 20-ml PE-bottle has been assumed to be constant for each element during the experiment. All reported U, Pu and Tc values have been corrected for adsorption.

3. Experimental procedure

3.1. Start-up

The experiment began two weeks after the MOX fuel was cut. During this time, the fuel was kept under N_2 atmosphere (<2% O_2). Prior to the start of the corrosion experiment and outside the hot cell, the autoclave was washed several times with mQ-water. Inside the hot cell, the two fuel fragments (B4 and B5, in Fig. 1(b)) were loaded into the autoclave fuel holder. Detachable fuel particles and possible pre-oxidized U(VI) present on the fuel surfaces were removed by washing the autoclave fuel holder containing the fuel fragments with 103.5 cm^3 of H_2 purged leachant, for a period of 30 min. After this, the fuel was immediately lowered into the autoclave containing 180 cm^3 of H_2 purged leachant. The leachant in the autoclave was continuously purged with H_2 gas during the loading procedure to avoid air oxygen presence. The assembling of the autoclave lid took 20 min. After this, the autoclave was pressurized with H_2 to 5.3 MPa. The fuel surface to leachant volume ratio at the start of the experiment was 0.282 m^{-1}. The entire experiment was run at a temperature of 23 ± 4 °C.

3.2. The corrosion experiment

The experiment was run for a period of 2078 days without interruption. The leachant was stirred with a titanium coated magnetic stirrer at a speed of 100 rpm during the first 180 days.

To examine the influence of different H_2 overpressures, a controlled decrease of the H_2 pressure to 0.1 MPa was made on day 1283. This was followed by a pressure increase to 0.3 MPa on day 1848 and a total gas exchange from pure H_2 to pure Ar on day 2011. After the gas exchange procedure, during which the gas-phase was exchanged 10 times to remove all H_2, the Ar overpressure was left at 0.35 MPa.

The autoclave was sampled empty on solution on day 1674. A refill of new solution was made on day 1848, i.e., as soon as the refill setup (see Fig. 2) was operational. In the time between day 1674 and 1848, the fuel was positioned above the leachant surface. To avoid air oxygen contamination and to establish similar conditions in the refill-leachant as in the experiment autoclave, the refill-leachant was conditioned with H_2 in the refill autoclave before the transfer. The conditioning and oxygen removal was achieved by five consecutive H_2 pressurizations and de-pressurizations (0 to 1 MPa) followed by 5 min of H_2 sparging. Following the conditioning of the leachant, the transfer line was purged with H_2 and a single batch of 103 cm^3 leachant was transferred. A second refill was made on day 2078 following the same procedure but with Ar as purging and conditioning gas instead of H_2. In this second refill, 135 ml leachant were transferred. The loss of water to the gas phase could be determined on day 1674 after the autoclave was sampled empty. This loss has been corrected for in the results.

Two experimental problems were encountered during the 5-year experiment. First, air oxygen accidentally entered the autoclave during H_2 refill after leachant sampling on days 492 and 734. Second, a leaking valve resulted in loss of H_2 from the experiment autoclave with a leak rate of 10 kPa/h, on day 1270. This leakage was stopped during sampling on day 1283.

4. Results

4.1. Corrosion experiment

The measured U and Cs concentrations, the calculated dissolved H_2 concentration together with the calculated total amount of released Cs as a function of time are plotted in Fig. 3. The U and Cs concentrations have been selected as 'system typical' parameters since they represent the main redox sensitive and insensitive constituents of the fuel, respectively. Hence, trends in U and Cs concentrations are expected to represent most species in the system. The H_2 concentration is a system parameter connected to the redox conditions of the leachant.

Four time regions are indicated at the top of Fig. 3. These represent periods with different conditions in the experiment. Region 1 includes the initial fuel dissolution and subsequent U reduction during the first 500 days. This region is characterized by a constant dissolved H_2 concentration of 42 mM. In region 2, ranging from day 500 to 1000, fuel oxidation is observed. This is due to air contamination of the H_2 supply line (see Section 3.2). Region 3, in the interval between day 1000 and 1600, is characterized by H_2 pressure reduction. Region 4 starts on day 1600 and lasts until the end of the experiment. This period includes a leachant refill, a corrosion period under H_2, followed by the gas exchange from H_2 to Ar and subsequent corrosion under Ar.

Region 1: The U concentration in the fresh leachant was measured to be 1×10^{-10} M. The three orders of magnitude increase (5×10^{-7} M) in the first sample taken 210 min after the start-up indicates the rapid dissolution of a pre-oxidized fuel layer. The oxidized U was quickly brought into solution by carbonate in the leachant. The U concentration in the first sample indicates that about 100 atomic layers were dissolved very rapidly. It is interesting to note that during these initial 210 min the amount of dissolved Cs

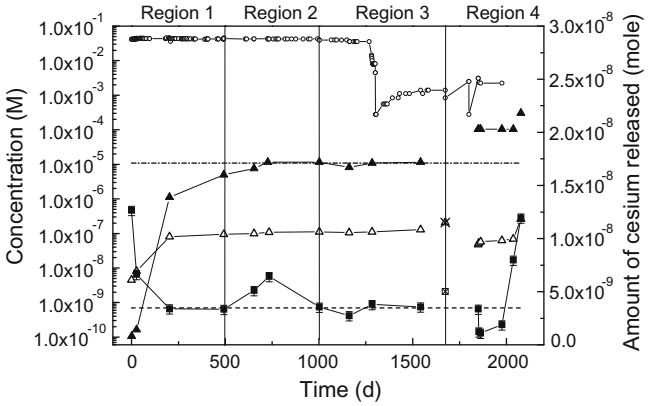

Fig. 3. Concentration of: U (■), Cs (Δ) and dissolved H_2 (○) and amount of released Cs (▲) as a function of corrosion time. The horizontal dashed line indicates a concentration of 7×10^{-10} M and the dash-dotted line at an amount of 1.71×10^{-8} mole. The error bars in the Cs concentration (±4%) are smaller than the data symbols in this logarithmic scale.

and other fuel nuclides indicate a congruent dissolution of the fuel (see Section 5.1).

During the following 203 days, the U concentration fell almost 3 orders of magnitude to 7×10^{-10} M. In the period between day 203 and 492, i.e., during 289 days, the concentration of U remained constant at a level of 7×10^{-10} M. Despite the decrease and stabilization of U concentration between days 1 and 492, the amount of dissolved Cs slightly increased from 1.4×10^{-8} M to 1.7×10^{-8} M. This is interpreted as due to slow exposure to new grain-boundary surfaces (see Section 5.1). But, it is also possible that parts of the Cs release are due to matrix dissolution or to depletion of the surface layer on Cs.

Region 2: Air intrusion on days 492 and 734 (see Section 3.2) led to oxidation of the fuel surface. This is indicated by an increase in U concentration and in the amount of released Cs. If congruent dissolution of pristine fuel is assumed during the two oxidations, the peak concentration of U can be calculated. Using the increase in Cs amount and the Cs to U ratio in the fuel of 8.1×10^{-3}, as obtained from the ORIGEN calculation, the maximal concentrations of U were determined to be 5×10^{-7} M after day 492, and 1×10^{-6} M after day 653. Despite this high calculated U concentration after day 653, the measurement on day 734 showed that an efficient reduction had taken place and that the concentration had decreased to 6×10^{-9} M.

On day 1002, the U concentration reached again the stable level of 7×10^{-10} M attained before air intrusion. It should be noted that during the reduction of the U no additional amounts of Cs were released from the spent fuel.

Region 3: It is characterized by steady state conditions without any measurable oxidative dissolution of the fuel. As a result, a stable U concentration is obtained in the leachant at 7×10^{-10} M (shown as a dashed line in Fig. 3).

A Cs plateau is established at 1.7×10^{-8} mole (dash-dotted line in Fig. 3) indicating that no new Cs is released from the fuel in this region. The total amount of Cs released during the first 1542 days of experiment corresponds to a fraction of 1.2×10^{-3} of the fuel inventory.

In the middle of this region, on day 1270, the H_2 concentration decreased from 42 mM to 6.4 mM during a 13 day period due to a leaking valve (see Section 3.2). The leak ended on day 1283 during solution sampling; the H_2 overpressure was then manually lowered to give a dissolved concentration of 0.8 mM. It can be concluded that a change of the H_2 concentration from 42 mM to around 1 mM, did not affect the U concentration in solution. Consequently, a concentration of 1 mM dissolved H_2 is enough to inhibit any dissolution of pristine fuel.

At the end of region 3, the autoclave was emptied on leachant during sampling. Unfortunately, the last sample point, from day 1674, was contaminated in the hot cell. This could be seen both by γ-spectrometry, in which ^{60}Co appeared for the first time, and in ICP–MS measurements showing elevated amounts of both actinides and lighter elements (the corresponding measured U and Cs concentrations are included in Fig. 3 as over-crossed symbols).

The released amount of Cs plotted in Fig. 3 (right scale) represents the total amount of dissolved Cs at each aliquot sampling, i.e., the sum of the amount in all aliquots removed from the autoclave plus the amount dissolved in the leachant inside the autoclave. Since the amount of Cs dissolved inside the autoclave depends on the remaining leachant volume, correction for water-loss due to evaporation to the dry gas-phase has been carried out.

Region 4: Once the refill autoclave was operational, on day 1848, a batch of 103 ml fresh leachant was transferred (see Section 3.2) and the H_2 concentration was increased to give 2.8 mM dissolved H_2.

At the end of the sampling on day 1674, a minute-long period with gas contact between the autoclave and hot cell atmosphere elapsed due to lack of leachant in the autoclave. During this time, significant amounts of air oxygen entered the autoclave. This led to oxidation of the fuel surface as seen by the large increase in dissolved Cs. The amount of Cs dissolved, between the last sample before and the first after the refill, was calculated to be 3×10^{-9} mole. This corresponds to a dissolution of 400 atomic layers of pristine fuel matrix, and a U concentration in solution of 3×10^{-5} M. Unfortunately, sampling directly after the refill to verify the high U concentration was not possible.

Despite the indications of oxidation, the leachate sampled two days after the refill had a U concentration of 6.5×10^{-10} M, i.e., the same concentration as before the refill. The concentration dropped an additional order of magnitude during the first two weeks after the refill. It is not known why this happened, but it is judged that the measured concentrations are correctly evaluated. Comparable U concentrations have recently been measured in a similar system. The dataset from this parallel experiment is, at the moment, under evaluation and indicates that the low concentrations are of major importance for the understanding of the H_2–MOX–H_2O system.

After the exchange of gas-phase to Ar on day 2011 (see Section 3.2), the U concentration increased rapidly. The leachate sampled on days 2037 and 2078 contained U concentrations of 2×10^{-8} M and 3×10^{-7} M, respectively. Also Cs was released during the corrosion under Ar atmosphere, indicating dissolution of pristine fuel matrix. Nevertheless, as the Np/U ratio measured under Ar atmosphere (shown in Table 5) is significantly lower than both the fuel inventory and the ratio day one, a large part of the concentration increase originates in dissolution of the previously precipitated UO_2 phase. Similar preferential oxidation of the precipitated phase has been observed before in experiments with UO_2 fuel [8,19].

4.2. Actinides

The Pu content in the MOX fuel decreased during irradiation from 4.92 to 3.54 wt%, at the same time the Pu composition changed towards heavier isotopes, i.e., ^{240,241,242}Pu. Neutron capture in these heavier Pu isotopes resulted in a build-up of Am and Cm. Since Am and Cm have a low mobility in the fuel most of the Am and Cm is expected to be found in the Pu-rich agglomerates in the spent MOX fuel.

In contrast, 85 at.% of the Np inventory (at the start of the experiment and based on the ORIGEN calculation) is found in the UO_2 matrix due to in-pile decay of ^{237}U. Only about 15 at.% of the Np is located in the Pu agglomerates due to α-decay of ^{241}Am. Even though this fraction will increase with time until all ^{241}Am has decayed, Np could be considered as representative of UO_2 matrix dissolution during this experiment.

The concentration of Np, Pu and Am as a function of corrosion time is shown in Fig. 4. It can be concluded that the trends for Tc, Pu and U are strongly correlated and that the Np measurements, at least, indicates a correlated behaviour. It can be speculated whether the U and Pu concentrations are decreasing through the same mechanism or if the decrease in Pu is a result of the decrease in U. A co-precipitation of actinide oxides seems most probable, since e.g. Np concentrations are several orders of magnitude lower than the solubility of Np(IV) oxide.

The higher dissolution rate of U compared with Pu during the air oxidation of the fuel (region 2), indicates that U is released preferentially during oxidative dissolution of the matrix as compared to Pu. This conclusion is also supported by the faster U dissolution compared with Pu under Ar atmosphere (region 4, days 2011 to 2078). Throughout stages of the experiment with concentration decrease, the Pu to U behaviour is harder to elucidate and further experiments are needed before a final understanding is obtained. However, there are indications at the beginning of region 1 and

Table 5
Ratio between the amount of dissolved Np, Pu and Am (mole), and the amount of dissolved U (mole) at different stages of the experiment.

	In fuel	ORIGEN	Wash	Day 1	H_2[a]	Ar[b]
Np	4.9×10^{-4}	3.5×10^{-4}	4.8×10^{-4}	4.8×10^{-4}	2.1×10^{-3}[c]	2.3×10^{-5}
Pu	3.4×10^{-2}	3.3×10^{-2}	4.4×10^{-4}	6.1×10^{-3}	8.9×10^{-2}	4.1×10^{-3}
Am	3.6×10^{-3}	4.7×10^{-3}	2.5×10^{-5}	5.8×10^{-4}	2.9×10^{-3}[b]	5.2×10^{-4}

[a] Average of samples from days 203, 492, 1002, 1161, 1283 and 1542.
[b] Value from day 2078.
[c] Values with a large uncertainty (±300%).

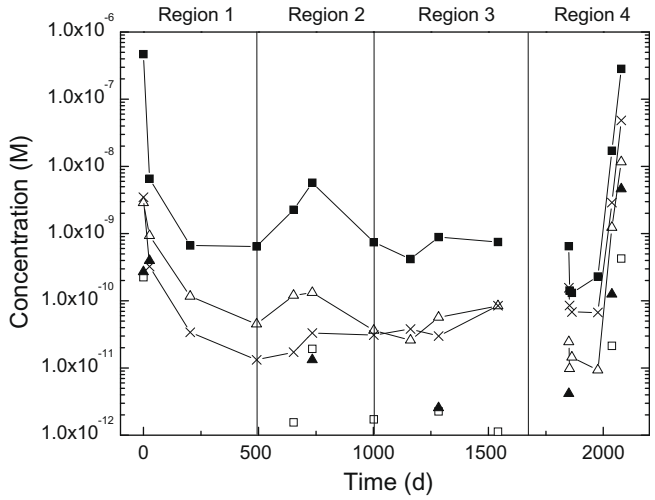

Fig. 4. The concentrations of: Np (□), Pu (Δ), Am (▲) and Tc (×) in solution as function of time. The U concentration (■) and the four regions from Fig. 3 are included for comparison. For clarity, the error bars for Pu and Tc have been omitted from the figure. The relative error in the Pu and Tc values is estimated to be ±60%.

during the decrease after day 734 that the U concentration decreases faster than Pu.

Owing to the fact that in most measurements the amounts of Np and Am were below the ICP–MS detection limit, Fig. 4 contains few data points for these minor actinides. The Np and Am data could not be corrected for sorption since they were not detected during the sorption study (see Section 2.7). The reported Am and Np data between day 500 and 2000 have large uncertainties as a result of the low concentration. Nevertheless, these data points are included to indicate that Am and Np release correlates reasonably well with their fuel inventories.

The ORIGEN calculation, based on the fuel inventory obtained from chemical analysis, reproduces well the Np/U, Pu/U and Am/U ratios found in the MOX fuel (Table 5). In the wash leachate, the Pu/U and Am/U ratios are smaller than expected for congruent fuel dissolution whereas the Np/U ratio is similar to the one found in the fuel. Similar observations have been reported in literature [36]. The same relations between the ratios in the leachate and in the fuel are seen also in the first autoclave sample (denoted as day 1 in Table 5).

The irradiated Pu agglomerates contain around 13 wt% Pu (Pu/U ~ 0.2), and the surrounding UO_2 matrix about 2 wt% Pu (Pu/U ~ 0.02) [28]. The Pu/U ratio measured in the leachate from day one (0.006) shows that U must be selectively oxidized and dissolved from the fuel. Moreover, as the matrix-associated Np/U ratio in the day one sample correlates well with the 'in fuel' inventory, whereas the Pu agglomerate-associated Pu/U and Am/U ratios in the same sample show underrepresentation of Pu and Am in solution, the oxidation and dissolution is believed to take place mainly on the UO_2 matrix.

At stable conditions under hydrogen (H_2 column in Table 5) only Pu and U are detectable with reliable accuracy. Under these conditions, Pu is found in a larger fraction (0.089) in the leachate than expected from the fuel inventory (0.034).This apparent accumulation of Pu in solution may be caused by the faster reduction of the U out of the solution. Another reason may be that the solution composition reflects equilibrium with a $(U–Pu)O_2$ co-precipitate formed after the reduction of oxidized species released during the dissolution of the pre-oxidized fuel layer.

Under Ar on day 2078, Np, Pu and Am were again measurable. This implies oxidation of the fuel surface. However, the relative amounts of actinides to U are lower by a factor of 10 than expected from the fuel inventory showing that oxidation of U is favoured.

4.3. Lanthanides

All leachates were analyzed for their contents of La, Ce, Pr, Nd, Sm, Eu, Gd, Tb and Dy. In presence of H_2 the lanthanides were detectable only in the leachate collected during the first day. Once the gas phase in the autoclave was changed from H_2 to Ar, Eu was detected by γ-spectrometry. The concentration of ^{154}Eu in the leachate on days 2037 and 2078 were 2.7×10^{-12} M and 2.7×10^{-11} M, respectively.

4.4. Transition metal inclusions

Technetium is associated with *4d* transition metal inclusions in the fuel [12,37]. The inclusions are formed during irradiation and are composed of Mo, Ru, Tc, Pd, and Rh. Generally, their size increases with increasing burn-up and irradiation temperature, and is in the range of 10 to 100 nm in a fuel with a burn-up of 45 GWd/tHM [29]. The inclusions are found at the grain boundaries rather than in the grains, and due to the higher burn-up, they are more frequent in the rim region than the centre of the fuel. The average composition of the particles in the rim of a 42 GWd/tHM MOX fuel has been reported to be; 16 wt% Mo, 7 wt% Tc, 34 wt% Ru, 8 wt% Rh and 35 wt% Pd [30].

The ICP–MS analyses of the leachates revealed the presence of natural Mo. After correction of the total Mo signal, no fingerprint of fission Mo was obtained. Fission Rh can not be distinguished from natural Rh as only one stable isotope, ^{103}Rh, exists. The remaining Rh isotopes are all short-lived and were extinct in the fuel. Ru and Pd were both present at or below the detection limit of $1 \cdot 10^{-11}$ M. Thus, Tc is the only *4d* transition metal that could be measured in the leachates. The Tc concentration in the leachates is shown together with the actinides in Fig. 4.

As the average burn-up in the UO_2 matrix was 13 GWd/tHM it may be concluded that the Tc in the leachates originate mainly from the high burn-up Pu agglomerates. Most likely, the corrosion of the metal inclusions found at the grain boundaries in the agglomerates is not related to agglomerate grain dissolution.

During the initial fuel oxidation on day 1, Tc was dissolved to a higher degree than expected from the fuel average $((Tc/U)_{leachate}/(Tc/U)_{fuel} \sim 3)$. During the first 200 days after this initial oxidation, the Tc concentration dropped two orders of magnitude to 3 ×

10^{-11} M. Thereafter, the concentration remained within the range $1–8 \times 10^{-11}$ M throughout the remaining period under H_2 atmosphere. Owing to the relatively constant Tc concentration and to the variations in the U concentration, the ratio $(Tc/U)_{leachate}/(Tc/U)_{fuel}$ changed between 2 and 200 during the period with H_2 overpressure. This indicates that Tc is easier to oxidize, and more difficult to reduce than U.

Under Ar atmosphere, the Tc concentration increased. However, the Tc/U concentration ratio decreased from 0.29 to 0.17, which implies that U was dissolved faster than Tc.

4.5. Radiolysis/hydrogen peroxide

The theoretical production rate of oxidizing H_2O_2 can be calculated using the inventory of the MOX fuel, the surface area of the fuel fragments, and tabulated [38] G-values (escape yields of radiolytically formed species as a function of the linear energy transfer of the emitted α-particles). This method of calculating the theoretical production rate of H_2O_2 yields 2×10^{-8} mole/day for our system.

Assuming that no H_2O_2 has reacted with the fuel matrix, the leachant is expected to contain 5×10^{-4} M H_2O_2 after 1674 days of fuel-water contact. The spectroscopic determination of H_2O_2 in the leachate from day 1674 gave a concentration below the practical detection limit of 1×10^{-6} M, reviling that almost all the H_2O_2 had been consumed in the system.

5. Discussion

Since it was shown that no accumulation of radiolytically produced H_2O_2 occurred in the leachant, the H_2O_2 must have reacted with the fuel surface. The calculated production rate of H_2O_2 is high enough to bring the concentration of U in the leachant to 1×10^{-6} M within 10 days. However, the U concentration remained at 7×10^{-10} M for several years under in presence of dissolved H_2. Consequently, spent MOX fuel corrosion in the presence of dissolved H_2 shows the same low dissolution of U as has previously been observed for spent UO_2 fuels (see Table 1). By changing the atmosphere to Ar, an increase in U concentration by several orders of magnitude was observed. Evidently, this is caused by the large amount of oxidants produced by the strong radiation field of the MOX fuel.

In the following paragraphs the experiment is discussed in terms of redox behaviour of the measured elements, reaction kinetics and relevance of the MOX fuel studied.

5.1. Caesium as matrix dissolution indicator

Caesium is present in the fuel at the grain boundaries and in the grains. The fraction located at grain boundaries is expected to be easily dissolved once contacted with water. Table 6 shows the ratio between amount of dissolved Cs and amount of dissolved U at different stages of the experiment.

If the ratio from the total dissolution test (in the fuel) is compared with the ratio released in the wash fraction, it is seen that Cs has been released to greater extent in the wash than would have been the case for congruent dissolution. On the other hand, if the ratio measured in the leachate on day 1 is compared with the fuel ratio, a good agreement is seen. This shows that the Cs release, mainly, is due to matrix dissolution from day 1 of the experiment, and that the 30 min of wash prior to the start-up was enough to remove nearly all Cs found at the grain boundaries on the fuel surface. Nevertheless, as previously mentioned (see Section 4.1, region 1) slow Cs release is taking place throughout the first year of the experiment, despite the reduction of U from the leachant; this open questions concerning the role of Cs as matrix dissolution indicator.

A similar behaviour of increasing Cs release, with decreasing dissolution rate over 140 days despite a falling U concentration, has been seen by Albinsson et al. in an experiment with UO_2 fuel (burn-up 41 GWd/tHM) [9]. This indicates that the slow release of Cs over long times is not a specific characteristic of MOX.

It is believed that the Cs release is due to exposure of water to new grain-boundary surfaces, which causes a delayed (instant) release. The Cs in inter-granular positions is assumed to be a caesium uranate phase on grain boundaries. However, only a fraction of the Cs rich phase is available at the outermost surfaces of the fuel fragments. This fraction is expected to be quickly dissolved and, therefore, to be responsible for the instant release of Cs. During the first year, slow dissolution of the grain boundary phase around the outermost grains results in a continuing release of Cs. However, the Cs phase contains U, and its dissolution is controlled by the water accessing the grain boundaries. The U corrosion process eventually blocks the dissolution of the inter-granular phase and the Cs concentration reaches a steady value.

If this is assumed to be the mechanism, it can be concluded that Cs is an indicator of the dissolution of the grain boundaries rather than of the grains themselves. Nevertheless, as the grain boundaries are the first to be oxidized, Cs can be considered to be a suitable indicator of the overall corrosion process.

5.2. Redox sensitive species and Am in presence of dissolved H_2

Literature data of equilibrium concentrations for pairs of aqueous/solid species, together with the measured concentrations of Tc and redox-sensitive actinides from the experiment, are presented in Table 7.

Based on the comparison of the experimental and literature data for U and Pu concentrations, as given in Table 7, it can be concluded that the low concentrations of actinides and Tc in our system must originate from reduced species. As a result, the oxidation states of the species in the leachant are expected to be Tc(IV), U(IV), Np(IV), Pu(IV) and possibly Pu(III).

Am is expected to exist as Am(III) under the reducing conditions prevailing in our experiment. The measured Am concentration of 1×10^{-12} M in the experiment is far below the solubility limit concentration of 5×10^{-8} M as given by $Am(OH)_3(aq)$ in contact with $Am(OH)_3(s)$ [39].

The very low Tc, Np and Am concentrations in the experiment is thought to be due to their low relative abundance in the fuel matrix. If an ideal solid solution is assumed (cf. results of Np/U mixtures in [40]), the measured 1×10^{-12} M Np concentration can be explained. Nevertheless, the measured Tc and Am concentrations are still one order of magnitude lower than explainable by their average abundance. This shows that they are originating from a phase with lower enrichment than the fuel average, which fits well with the previous conclusion that the corrosion of the MOX surface mainly takes place on the low burn-up UO_2 matrix.

5.3. Kinetics of the reduction reaction

System-independent rate constants assuming zero, first and second order reactions for the reduction rate were calculated based on the fuel surface area (50.8 mm^2), and the U concentration together with solution volume at three stages of the experiment:

Table 6
Ratio between the amount of dissolved Cs (mole) and the amount of dissolved U (mole) at different stages of the experiment.

In fuel	ORIGEN	Wash	Day 1	H_2[a]	Ar
8.1×10^{-3}	7.4×10^{-3}	6.8×10^{-2}	9.7×10^{-3}	1.6×10^{2}	9.12×10^{-2}

[a] Average of samples from days 203, 492, 1002, 1161, 1283 and 1542.

Table 7
Comparison between measured and reported values for Tc and actinide concentrations under reducing condition. The reference U and Pu concentrations (reducing conditions; Red.) were measured in systems without carbonates; the U was measured at an elevated temperature of 100 °C. The abundances in fuel given are based on the calculated (ORIGEN) number of moles of each element in relation to total number of moles of actinides and fission products.

	Abundance in fuel (mole%)	Concentration (M)			Corresponding phases (lit.)	Reference
		H_2 (exp.)	Ar (exp.)	Red. (lit.)		
Tc	0.25	3×10^{-11}	4×10^{-8}	8×10^{-8}	$TcO_2 \cdot nH_2O(s)/Tc(OH)_2CO_3(aq)$	[46]
U	87.5	7×10^{-10}	3×10^{-7}	3×10^{-10}	$UO_2(s)/U(OH)_4(aq)$	[47]
Np	0.03	1×10^{-12}	4×10^{-10}	5×10^{-9}	$Np(OH)_4(s)/Np(OH)_4(aq)$	[48]
Pu	2.9	5×10^{-11}	1×10^{-8}	3×10^{-11}	$PuO_2(s)/Pu(OH)_4(aq) + Pu(OH)_3(aq)$	[49,50]

(i) at the beginning of region 1; (ii) after the air ingress in region 2–3; and (iii) in the beginning of region 4.

The number of data points useable for reaction rate calculation is too sparse to obtain an unambiguous determination of the reaction order. The results show fairly consistent values for both zero- and first-order reaction rate constants, but exclude higher order reactions. The average constant for a zero-order reaction was calculated to $k_{zero} = 10^{-15}$ mol/(m^2 × s) and for a first-order reaction to $k_{first} = 10^{-6}$ m/s. Further experiments are needed before a better determination can be made.

5.4. Argon atmosphere

The fuel oxidation and dissolution under Ar did not proceed as fast as the theoretical radiolytic production of oxidative species suggests. The expected production rate of H_2O_2 in the system of 6×10^{-7} mole/day (see Section 4.5) is not consistent with the increase in the actinides (7×10^{-11} mole/day) in the leachant between day 2037 and 2078. Consequently, the fuel continued to be, at least partly, protected against oxidation after the atmosphere was changed. Such memory effect of previous H_2 atmosphere has been seen in other experiments on irradiated fuels [41] and UO_2(s) containing metallic Pd particles [42].

A plausible explanation is that H_2 released from the autoclave walls after the change of atmosphere gives a concentration of dissolved H_2 near the fuel surface high enough to decrease the oxidation rate.

5.5. UO_2/MOX comparison

An important difference between MOX and UO_2 fuels is the fission density. In a UO_2 fuel, the $^{235}UO_2$ enrichment is homogenously distributed in the $^{238}UO_2$ fuel matrix, resulting in an initial even fission density in the entire matrix. In contrast, in MOX fuel the fissile nuclides are concentrated in the highly enriched Pu agglomerates. In the MOX fuel about 75% of fission takes place in these agglomerates resulting in a local burn-up up to 270 GWd/tHM for a MOX fuel with an average burn-up of 44.5 GWd/tHM [28].

It is seen from our results that MOX fuel, despite this difference, behaves very similarly to irradiated UO_2 under the corrosion conditions studied. The stable concentration of U in our experiment (7×10^{-10} M) is in the range, or even lower, than that reported for UO_2 fuels (see Table 1). The Pu concentration in the experiment (5×10^{-11} M) is a factor of 2 higher than has been reported from UO_2 fuel with similar burn-up [8]. This might be explained by the larger Pu fraction available on the surface of the MOX fuel.

The results of this study indicate that oxidation and dissolution of the MOX fuel, mainly, takes place in the $^{238}UO_2$ matrix where the burn-up is low (13 GWd/tHM).

5.6. Relevance of fuel

As described in the fuel chapter above (see Section 2.1), the MOX fuel used in this experiment is of OCOM 30 type, produced in 1986. Since then, MOX fabrication has been improved by the introduction of the micronized master blend process, MIMAS, which is now used for most MOX fuels on the market.

The difference between the OCOM and MIMAS processes lies in the production of the Pu agglomerates. In the MIMAS, the micronization (crushing) of the UO_2 and PuO_2 powder gives a more uniform dispersion of the plutonium in the agglomerates, which promotes the formation process of a $(U–Pu)O_2$ second phase during sintering. This is an advantage during reprocessing due to better dissolution properties in nitric acid [20]. Nevertheless, the final product in both processes is a 30% PuO_2 enriched UO_2 master mix, which is blended (without milling) with natural UO_2 to give a Pu concentration in the MOX fuel of about 5% [43]. As a consequence, both processes results in a heterogeneous fuel with the fissile material located in Pu agglomerates.

Since the expected difference between MOX and UO_2 fuels would be related to the heterogeneity of the MOX structure, the results of this study, performed on a highly heterogeneous MOX, is expected to be representative for all heterogeneous MOX fuels.

6. Conclusions

The study showed that the presence of H_2 inhibits the corrosion of MOX fuel. At H_2 concentrations in the range 1–42 mM, the leachant concentration of U remained stable at 7×10^{-10} M, Pu stabilized at 5×10^{-11} M, whereas Np and Am were measured at the detection limit of 1×10^{-12} M. Tc originating from dissolution of *4d* metal particles was found at a stable concentration of 3×10^{-11} M. Based on these concentrations, redox sensitive elements such as Tc, Np, U and Pu are expected to be found in tetravalent state in the leachant.

In our system, Pu was found to be less sensitive to oxidation than U.

Caesium was released during the first two years of experiment as a response to slow exposure of new grain-boundary surfaces to water. More than 80% of this release occurred during the first 200 days. After the first two years, no more Cs was released form the fuel in the presence of hydrogen.

The results indicate that it is mainly the UO_2 matrix of the MOX fragments that is oxidized and that corrosion of the highly burnt Pu agglomerates is relatively small. This is expected to be the case for all heterogeneous MOX fuels.

Based on these results, under reducing conditions no difference between the corrosion behaviour of MOX fuel and UO_2 fuel of similar burn-up is expected.

Acknowledgements

We would like to thank H. Panissie, H.-M. Stutz and F. Blattmann in the design office and mechanical workshop. Many thanks to D. Baudot, D. Papaioannou, E. Toscano and J.-L. Arnoult for their help with the fuel. The hot cell team; E. Teixeira, M. Cardinale, A. Walschburger, S. Birck, B. Lynch and B. Christiansen are gratefully acknowledged. Further we would like to thank Dr W. Goll, Areva

NC, for the allowance to use the irradiated MOX fuel and for the complementary fuel data. Thanks are also due to P. Peerani for performing the ORIGEN calculations and J.-P. Glatz, V.V. Rondinella, C.T. Walker and T. Gouder for their critical reviews of the paper. Finally, we would like to thank the anonymous reviewers for valuable comments.

References

[1] SKB Technical Report 92-20, Swedish Nuclear Fuel and Waste Management Co., Stockholm, 1992.
[2] SKB Technical Report 99-06, Swedish Nuclear Fuel and Waste Management Co., Stockholm, 1999.
[3] L. Johnson, C. Ferry, C. Poinssot, P. Lovera, J. Nucl. Mater. 346 (2005) 56.
[4] I. Puigdomenech, L. Trotignon, S. Kotelnikova, K. Pedersen, L. Griffault, V. Michaud, J.-E. Lartigue, K. Hama, H. Yoshida, J. West, K. Bateman, A. Milodowski, S. Banwart, J. Rivas Perez, E-L. Tullborg, Mat. Res. Soc. Symp. Proc. 608 (2000) 179.
[5] B. Bonin, A. Colin, A. Dutfoy, J. Nucl. Mater. 281 (2000) 1.
[6] L. Liu, I. Neretniks, Nucl. Technol. 138 (2002) 69.
[7] A. Loida, V. Metz, B. Kienzler, H. Geckeis, J. Nucl. Mater. 346 (2005) 24.
[8] K. Spahiu, D. Cui, M. Lundström, Radiochim. Acta 92 (2004) 625.
[9] Y. Albinsson, A. Ödegaard-Jensen, V.M. Oversby, L.O. Werme, Mater. Res. Soc. Symp. Proc. 757 (2003) 407.
[10] S. Röllin, K. Spahiu, U.-B. Eklund, J. Nucl. Mater. 297 (2001) 231.
[11] K. Spahiu, L. Werme, U. Eklund, Radiochim. Acta 88 (2000) 507.
[12] H. Kleykamp, J. Nucl. Mater. 131 (1985) 221.
[13] M.E. Broczkowski, J.J. Noel, D.W. Shoesmith, J. Nucl. Mater. 346 (2005) 16.
[14] S. Nilsson, M. Jonsson, J. Nucl. Mater. 372 (2008) 160.
[15] M. Jonsson, F. Nielsen, O. Roth, E. Ekeroth, S. Nilsson, M. Hossain, Environ. Sci. Technol. 41 (2007) 7087.
[16] E. Cera, J. Bruno, L. Duro, T Eriksen, SKB Technical Report 06-07, Swedish Nuclear Fuel and Waste Management Co., Stockholm, 2006.
[17] T. Eriksen, M. Jonsson, J. Merino, J. Nucl. Mater. 375 (2008) 331.
[18] B. Muzeau, C. Jégou, F. Delaunay, V. Broudic, A. Brevet, H. Catalette, E. Simoni, C. Corbel, J. Alloy. Comp. 467 (2009) 578.
[19] P. Carbol, J. Cobos-Sabate, J.-P. Glatz, C. Ronchi, V. Rondinella, D.H. Wegen, T. Wiss, A. Loida, V. Metz, B. Kienzler, K. Spahiu, B. Grambow, J. Quinones, A. Martinez, E. Valiente, SKB Technical Report 05-09, Swedish Nuclear Fuel and Waste Management Co., Stockholm, 2005.
[20] The Safety of the Nuclear Fuel Cycle, OECD Nuclear Energy Agency Committee on the Safety of Nuclear Installations, OECD Nuclear Energy Agency Working Group on the Safety of the Nuclear Fuel Cycle, OECD Nuclear Energy Agency, OECD Publishing, 2005, p. 34.
[21] D. Haas, D.J. Hamilton, Progr. Nucl. Energ. 49 (2007) 574.
[22] J.-M. Gras, R. Do Quang, H. Masson, T. Lieven, C. Ferry, C. Poinssot, M. Debes, J.-M. Delbecq, J. Nucl. Mater. 362 (2007) 383.
[23] A. Loida, B. Grambow, G. Karsten, P. Dressler, Mat. Res. Soc. Symp. Proc. 506 (1998) 923.
[24] J.-P. Glatz, P. Carbol, J. Cobos-Sabaté, T. Gouder, F. Miserque, J. Gimenez, D. Wegen, Mat. Res. Soc. Symp. Proc. 663 (2000) 449.
[25] C. Jégou, S. Peuget, V. Broudic, D. Roudil, X. Deschanels, J.M. Bart, J. Nucl. Mater. 326 (2004) 144.
[26] J. Quiñones, J. Cobos, E. Iglesias, S. van Winckel, A. Martínez-Esparza, J.-P. Glatz, in: Proceedings MOFAP '07, OECD/NEA, in press.
[27] C.T. Walker, W. Goll, T. Matsumura, J. Nucl. Mater. 245 (1997) 169.
[28] C.T. Walker, W. Goll, T. Matsumura, J. Nucl. Mater. 228 (1996) 8.
[29] H. Bailly, D. Ménessier, C. Prunier, The nuclear fuel of pressurized water reactor and fast neutron reactors, Lavoisier Publishing, Paris, 1999. p. 123.
[30] H. Kleykamp, J. Nucl. Mater. 324 (2004) 198.
[31] O.W. Hermann, C.V. Parks, NUREG/CR-0200, Oak Ridge, September 1998.
[32] F. Nielsen, M. Jonsson, J. Nucl. Mater. 359 (2006) 1.
[33] B.G. Santos, J.J. Noël, D.W. Shoesmith, J. Nucl. Mater. 350 (2006) 320.
[34] B.G. Santos, J.J. Noël, D.W. Shoesmith, Corrosion Sci. 48 (2006) 3852.
[35] C.J. Hochanadel, J. Phys. Chem. 56 (1952) 587.
[36] E. Ekeroth, J. Low, H.-U. Zwicki, K. Spahiu, Mat. Res. Soc. Symp. Proc. 1124 (2009) 1124-Q02-07.
[37] L. Thomas, R. Einziger, R. Woodley, J. Nucl. Mater. 166 (1989) 243.
[38] B. Pastina, J.A. LaVerne, J. Phys. Chem. A 105 (2001) 9316.
[39] R.J. Silva, G. Bidoglio, M.H. Rand, P.B. Robouch, H. Wanner, I. Puigdomenech, Chemical Thermodynamics of Americium, Elsevier Science Publishers, Amsterdam, 1995.
[40] D. Rai, N. Hess, M. Yui, A.R. Felmy, D.A. Moore, Radiochim. Acta 92 (2004) 527.
[41] K. Spahiu, U.-B. Eklund, D. Cui, M. Lundström, Mat. Res. Soc. Symp. Proc. 713 (2002) JJ14.5.1.
[42] M. Trummer, S. Nilsson, M. Jonsson, J. Nucl. Mat. 378 (2008) 55.
[43] R.J. White, S.B. Fisher, P.M.A. Cook, R. Stratton, C.T. Walker, I.D. Palmer, J. Nucl. Mater. 288 (2001) 43.
[44] R.S. Forsyth, L.O. Werme, J. Bruno, J. Nucl. Mater. 138 (1986) 1.
[45] Wolfgang Goll, AREVA NP GmbH, personal communication.
[46] J.A. Rard, M.H. Rand, G. Anderegg, H. Wanner, Chemical Thermodynamics of Technetium, Elsevier Science Publishers, Amsterdam, 1999.
[47] R. Guillaumont, T. Fanghänel, J. Fuger, I. Grenthe, V. Neck, D.A. Palmer, M.H. Rand, Update on the Chemical Thermodynamics of Uranium, Neptunium, Plutonium, Americium and Technetium, Elsevier Science Publishers, Amsterdam, 2003.
[48] R.J. Lemire, J. Fuger, H. Nitsche, P. Potter, M.H. Rand, J. Rydberg, K. Spahiu, J.C. Sullivan, W.J. Ullman, P. Vitorge, H. Wanner, Chemical Thermodynamics of Neptunium and Plutonium, Elsevier Science, Publishers, Amsterdam, 2001.
[49] V. Neck, M. Altmaier, Th. Fanghänel, J. Alloy. Comp. 444&445 (2007) 464.
[50] D. Rai, Y.A. Gorby, J.K. Fredrickson, D.A. Moore, M. Yui, J. Solution Chem. 31 (2002) 433.